Color Coronal Spectral Analysis: Results with Water Solution of Calcium Carbonate

Ignat Ignatov[1], Christos Drossinakis[2] and Alexander I. Ignatov[1]

[1*]*Scientific Research Center of Medical Biophysics, Sofia, Bulgaria*
[2]*IAWG- Internationale Akademie für Wissenschaftliche Geistheilung, Frankfurt, Germany; Marchegg, Austria*
Corresponding author: mbioph@abv.bg

Received 19/06/2023; accepted 10/12/2023
https://doi.org/10.4152/pea.2025430203

Abstract
In 2007, a study was done using color corona spectral analysis [39]. The method was applied in laboratory conditions with the coronal glow of biological objects and liquids. A high voltage of 12 kV and a frequency of 15 kHz have been applied during the research. In 1995, Antonov created the apparatus for the study, with registration in black and white photographic films. The scientist called the method selective high-frequency discharge. It has been categorized as silverless photography. In the presence of electrical conditions, electrography is at the heart of the photocopier invention. Herein, $CaCO_3$ in a distilled H_2O solution was tested. Comparative analysis was performed with distilled H_2O. Physical and chemical processes under high-frequency corona gas discharge conditions were analyzed. $CaCO_3$ was in dynamic interaction with CO_2 and H_2O at the boundary of different environments.

Keywords: $CaCO_3$; color coronal discharge; FTIR; H_2O.

Introduction•

Corona gas discharge produces a typical glow on devices with a 5 to 30 kV voltage and frequencies from 10 to 150 kHz [1]. In 1949, [2] received a patent for a "Method for obtaining photographic pictures of different types of objects".
The method of selective electric discharge allows for a dielectric medium to record information on another that is in contact with it. It is based on electric discharge at normal atmospheric pressure in a three-layer condenser: dielectric-air gap-dielectric [3, 4]. A constant and controllable by-force electric field is created in it. In certain places where the electric field surprises the breakdown value of the field in the air gap, a perforation in the last one occurs. Pashen's law [5] describes this phenomenon as:

$$V_B = f(pd) \quad (1)$$

V_B depends on p and d.
Due to perforation, electric discharge is selectively remitted on the recording electric medium.
In 1965, [6] has published an electrophotography book with corresponding technology for directly capturing corona discharges from biological objects,

• The abbreviations and symbols definitions lists are on pages 121-122.

especially around larger contact surfaces. Electrophotography is by far the most significant of all the reprographics technologies for photocopying and laser/LED printing.
In 1975, [7] have described the gas discharge effect with copying on the photographic photo film as electrophotography.
Since 1960, [8, 9] have developed electrophotographic methods for images registration.
In 1968, [4] has developed a method for gas discharge photography. [10-18] have also made researches in this area. During the process, in the ionization zone, sliding discharge develops on a dielectric surface powered by a non-uniform electric field near an electrode with a small curvature radius. The small gap thickness between the experimental object and the electrode ranges from 10 to 100 μm.
Experimentally, the gas discharge effect gives information on the electric field distribution in the air gap between the object and the registering medium during the discharge [1, 19-21]. Ions of N, O, CO_2 and free electrons form the discharge itself. The free electrons are separated from N_2, O_2 and CO_2 molecules, which generate gas discharge between the studied object and the electrode [22-24].
Research has focused on analyzing an insight conclusion about digital analysis on the corona gas discharge spectrum, by introducing a pre-processing procedure to extract the texture effects as the radiation energy signature based on its most significant glow (digitally imaged isolines), which is used for medical biometric and disease interpretations [25].
During corona gas discharge in the atmosphere, there is a process of CO_3^- formation [26]. When $CaCO_3$, H_2O and CO_2 are combined, the following reaction is observed [27].

$$CaCO_3 + H_2O + CO_2 = Ca(HCO_3)_2 \quad (2)$$

[28] have developed a gas discharge photography method that that described the reaction as:

$$CaCO_3 + HOH + CO_2 = Ca(HCO_3)_2 \quad (3)$$

Falk has shown that HOH bending is fundamental for solids and liquids [29].
$CaCO_3$ has the most extensive local extremums at 873 [30] and 1457 cm^{-1} [31].
Studies employing NES and DNES [33-35] methods with 873 cm^{-1} were made for cave water [32], the environment process [36] and plants with Ca^{2+} [36, 37].
The present investigation aimed to prove that, in coronal gas discharge conditions, there is an activation of the separated photons processes for $CaCO_3$ ions and H_2O reactions.

Materials and methods

Device for color coronal spectral analysis

Gas discharge emission for color coronal spectral analysis [1, 21, 23, 37, 38] was investigated in a dark room. It was registered with a photosensitive paper or color film placed on transparent Hostaphan electrode with an 87 mm diameter. It was filled with a conductive liquid composed of a 1% NaCl solution in deionized H_2O. Herein, the 1% solution was made from $CaCO_3$. Investigated objects (H_2O drops and human thumbs) were placed on the corresponding photosensitive

material. Pulses with 12 kV voltage and a carrier frequency of 15 kHz were applied between the objects and the electrode Cu coating.
The functional scheme of gas corona discharge device is shown in Fig. 1.

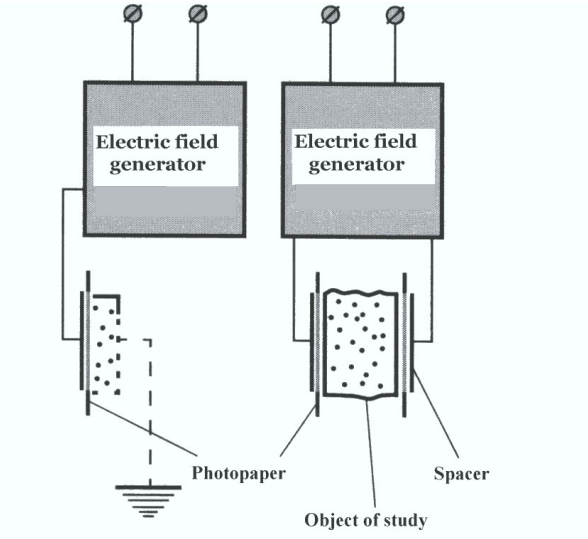

Figure 1: Functional scheme of gas corona discharge device.

Corona gas discharge was generated in the gap between the investigated objects and the transparent electrode, producing a characteristic glow around the contact area. Its electromagnetic emission, which ranged from 380 to 495 nm and 570 to 750±5 nm, illuminated the corresponding photosensitive material, according to the objects specific properties (Fig. 2) [39].

Figure 2: Transparent electrode with 87 mm diameter made of Hostaphan and filled with conductive liquid (1% $CaCO_3$ in a distilled H_2O solution).

Color images produced by visible, UV and IR radiation were processed and analyzed with a dedicated software package. Measured spectral characteristics were calculated in eV.

FTIR

IR-spectra of $CaCO_3$ were registered on a Brucker Vertex ("Brucker", Germany) FTIR (spectral range: average IR- 370 ÷ 7800 cm^{-1}; visible- 2500 ÷ 8000 cm^{-1}; permission- 0.5 cm^{-1}; accuracy of $\tilde{\nu}$ - 0.1 cm^{-1} on 2000 cm^{-1}) and Thermo Nicolet Avatar 360 FTIR spectrometers.

NES and DNES methods

θ was measured with a specially designed instrument, which has been described in detail by [40-43]. H_2O drops evaporation was performed in a sealed chamber with a stable temperature of 22 ºC and humidity from 65 to 70% [40, 43] (Fig. 3). The drops were placed on a 350 μm thick BoPET sheet.

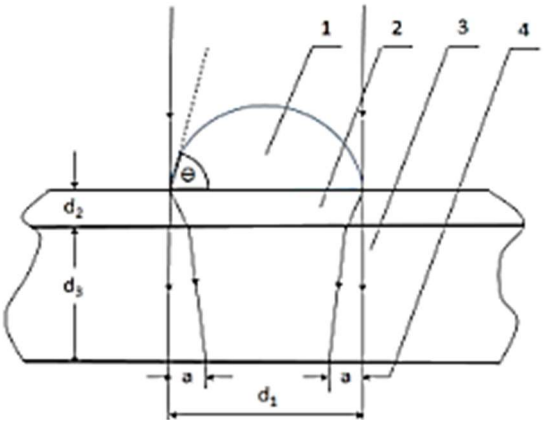

Figure 3: Operating principle of the method for measuring the liquid drops θ on a hard surface: 1- drop, **2**- thin Maylar sheet, **3**- glass plate and **4**- refraction ring width.

θ is a function of a and d_1.

The device had the following technical features: monochromatic filter with λ of 580±7 nm; H2O evaporation angle ranging from 72.3 to 0 deg; measured range of hydrogen bonds energy among H2O molecules was λ = 8.9 ÷13.8 μm or E = -0.08 ÷ -0.1387 eV.

Luck has considered that, in H_2O, hydrogen bonds exist between H atom of one H_2O molecule and O of another [44]. Most of them are bound by the connection energy (-E) and the remaining are free (E = 0). It is accepted that E has a negative value. This is known as Luck's two-state model [45-48]. The number of hydrogen bonds between H atom of one H_2O molecule and O of another in a volume of H_2O is twice as high as the number of molecules it contains.

Part of the hydrogen bonds is restructured in the proximity of the drop surface spherical part and which produces dependence between δ and hydrogen bond energy [49-51].

$$\delta = -kT/\ln[(1+\alpha)/(e^{-E/kT} + \alpha)] \quad (4)$$

where k is Boltzmann constant, E is hydrogen bond energy, α is the ratio of the phase space two sub-volumes related to hydrogen bonds (α = 28±8) structuring and restructuring, and I ($5.03.10^{18}$ m^{-2}) is H_2O molecules density in the hydrophobic surface layer. E and α values were determined by comparison with

the experiment. Expression (4) explains fraction C as $\delta = C\gamma$ [50]. According to [43, 50], non-hydrogen bond interaction contribution amounts to 20% of γ and C real value (= 4/5). Considering Helmholtz free surface energy:

$$F = \gamma\Sigma \quad (5)$$

where Σ is the drop surface spherical part [43].
At the instant of mechanical equilibrium, F should be minimal, i.e., dF = 0 = d(γΣ) [43].

$$0 = \gamma\Sigma - \gamma_0\Sigma_0 \quad (6)$$

H_2O drops forced evaporation process occurs at a constant temperature of 20 ºC in a hermetic camera [40].
Expressions for Σ_0 and Σ are as follows [43]:

$$\Sigma = \pi D^2/2(1 + \cos\theta);\ \Sigma_0 = \pi D^2/2(1 + \cos\theta_0) \quad (7)$$

$$-E/kT = C\gamma/IkT \quad (8)$$

$$E = C\gamma o(1 + \cos\theta)/I(1 + \cos\theta_0) \quad (9)$$

During the process, θ changes in discrete steps and characterizes hydrogen bonds average E as follows:

$$\theta = \arccos(-1 + bE) \quad (10)$$

$$b = I(1 + \cos\theta_0)/C\gamma o \quad (11)$$

where b is a temperature-dependent parameter [52, 53]. The employed methods were NES and DNES [53-55]. They are used for research on natural waters [37, 53, 55], plants [35] and blood serum [56]. Molecular dynamics simulation was applied to investigate H_2O droplets wetting behavior on the sandstone surface under different salinities. The system equilibrium configuration was used for studying the interaction of its components. The number of hydrogen bonds was calculated [57, 58]. E of hydrogen bonds among H_2O molecules in H_2O samples is measured in eV. A non-equilibrium evaporation process of H_2O droplets characterizes f(E) of H_2O. NES is measured in eV^{-1}. DNES is defined as the difference [53-55]:

$$\Delta f(E) = f(H_2O \text{ sample}) - f(\text{control sample}) \quad (12)$$

DNES is measured in eV^{-1}, where f (*) denotes evaluated E [50-54].

Results

Parameters of 1% $CaCO_3$ in a distilled H_2O solution obtained by color coronal spectral analysis

Electric discharge per unit area of the recording medium can be expressed as follows [20]:

$$\sigma = [\alpha - U_p(d_2 + \delta)/d_2]\varepsilon_0(d_2 + \delta)/\delta d_2 \quad (13)$$

where $\delta = d_1/\varepsilon_1 + d_3/\varepsilon_3$; T is electric pulse duration; U_p is VB of the air gap between experimental object and recording medium; d_1, d_2 and d_3 are the

thickness of the object, air gap, and photosensitive material, respectively; ε_0 (1.00057 F/m^{-1}), ε_1 and ε_3 are dielectric permittivity of air, experimental object and photosensitive material, respectively.
VB of the air gap is:

$$U_p = 312 + 6{,}2d_2 \quad (14)$$

Consequently, a quadratic equation describing the width of the air gap is obtained:

$$6{,}2\, d_2^2 - (\alpha T - 6{,}2\delta - 312)d_2 + 312\, \delta = 0 \quad (15)$$

It has the following solutions:

$$d_2 = [\alpha T - 6{,}2\delta - 312] \pm [(\alpha T - 6{,}2\delta - 312)^2 - 7738\delta)^{1/2} \quad (16)$$

Coronal gas discharge method has applications for researching H_2O drops electrical parameters in gas discharge conditions [5].
The dielectric constant as a parameter of coronal gas discharge was described by [3, 10]. It is a reliable dielectric permittivity in a homogenous medium.
The object conductivity is not practically reflected in the formation of the electric image. The image gives information on the dielectric and geometrical object characteristics, dielectric permittivity distribution and surface unevenness [5, 9].
Dielectric permittivity is determined by the ability of a material to polarize due to an applied electric field, thereby partially neutralizing it in the material. Polarization refers to the displacement or orientation of associated electrical charges under the action of a field.
Investigation with the method of color coronal spectral analysis [1, 21, 22, 37, 38] was performed on the electric glow of the control sample (distilled H_2O) and 1% $CaCO_3$ in a distilled H_2O solution (Fig. 4).
The electrode from Fig. 2 was positively charged. The negative electrode was approached until a corona breakdown voltage occurred.

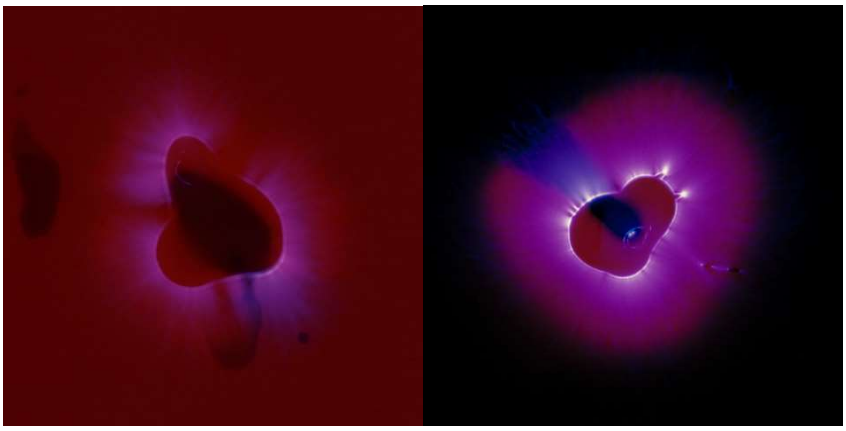

Figure 4: Color coronal images of the control sample (distilled H_2O) and of the specimen with 1% $CaCO_3$ in a distilled H_2O solution.

Fig. 4 illustrates that the photon emission for the control sample was E = 2.05 eV or λ = 605 nm, and the average outcome was in the Em orange range. The result for the

1% $CaCO_3$ sample was E = 2.98 eV or λ = 416 nm, i.e., the average outcome was in the Em violet range. The difference was E = 0.92 eV. H_2O drop radius was 0.41 cm or $S = \pi r^2$. $S = 3.14 \times 0.41^2 = 0.528$ cm^2.
For the control sample, the result was 2.11 eV/0.528 cm^2 = 4.00 eV/cm^{-2}. The result of the 1% $CaCO_3$ sample was 2.98 eV/0.528 cm^2 = 5.64 eV/cm^{-2}.
The outcome of a discharge at the liquid drops point of contact with the photo film is valuable. For distilled H_2O, V_B had 31% discharge with photons in the red Em, where E = 1.68 eV or λ = 738 nm. With 1% $CaCO_3$, there was 73% discharge with photons in the violet Em, where E = 3.02 eV or λ = 410.5 nm.
The method for brightness estimation from coronal discharge emission research was developed [19, 59].
The formula calculates P_{eff} of the device for color corona discharge:

$$P_{eff} = U^2/R \quad (17)$$

where U = 12 kV. Corona discharge for H_2O drop was $R = 10^9$ Ω. $P_{eff} = U^2/R = 12^2 10^6/10^9 = 0.144$ W.

Results with pH and electric conductivity

Table 1 shows the change of parameters for 1% (w/v) $CaCO_3$ after 30 sec corona gas discharge, where U = 12 kV and ν =15 kHz.

Table 1: Parameters for 1% $CaCO_3$ in a distilled H_2O solution with coronal gas discharge effect.

Parameters	Distilled H_2O	1% (v/v) $CaCO_3$	1% (v/v) $CaCO_3$ Gas discharge effect
Electric conductivity (μS/cm^{-1})	28.1 ±0.28	55.1 ±0.55	57.3 ±0.57
pH	7.51 ±0.75	9.07 ±0.09	9.33 ±0.09

There was an increase in the studied electric conductivity and pH values. The number of OH- hydroxyl groups also increased with higher pH values.
There was a statistically significant difference between the 1% $CaCO_3$ solution in distilled H_2O before and after the coronal effect, according to the Student's t-test at $p < 0.01$ level.

Results of reactions with $CaCO_3$

The research on $CaCO_3$ was performed with FTIR, which showed that the peaks at $\tilde{\nu}$ = 713, 873, 1457, 1627, 1793, 2512 and 3447 cm^{-1} [60, 61] (Fig. 5).
DNES of H_2O was studied from *Temnata dupka* (Dark hole) cave with Ca^{2+} and HCO_3^- contents of 66 and 223 mg/L^{-1}, respectively. A peak was observed at E = -0.1087 eV, λ = 11.41 μm and $\tilde{\nu}$ = 877 cm^{-1}. FTIR analysis of $CaCO_3$ had the following results: E = -0.1082 eV; λ = 11.46 μm; and $\tilde{\nu}$ = 873 cm^{-1}. H_2O vapor spectral range ranged from 0 to 877 cm^{-1} [62]. Adsorption peaks for $CaCO_3$ were at 713 and 875 cm^{-1}. The results indicate that an analysis of peaks at 713 and within the interval of 873 ÷ 879 cm^{-1} can be used to evaluate NES processes with $CaCO_3$ in H_2O and air. Since exposure to H_2O with different physicochemical parameters, air moisture, and thermal effects can be

assessed, the quality of $CaCO_3$ solutions and protection against CO_2 emissions is stronger.

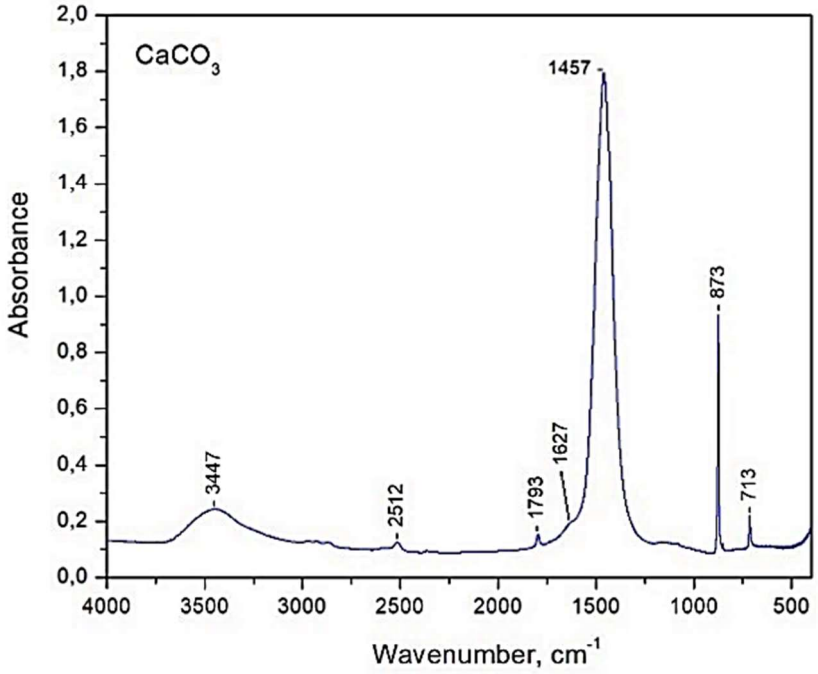

Figure 5: FTIR results for $CaCO_3$.

The present study illustrates an increase in f(E) peak at 877 cm^{-1}, from 32.6 to 39.9 eV^{-1}, during the process of coronal discharge on 1% $CaCO_3$ in a distilled H_2O solution (Table 2).

Table 2: Results for 1% $CaCO_3$ in a distilled H_2O solution before and after coronal discharge**.**

1% $CaCO_3$ in distilled H_2O	**1% $CaCO_3$ in distilled H_2O after coronal discharge f(E) with eV^{-1} of 877 cm^{-1}**
32.6	45.3
32.3	44.8
32.8	45.1
32.8	45.2
32.7	44.8
32.2	44.7
32.6	44.9
32.7	44.8
32.7	44.6
32.8	45.2
average result	average result
32.6	44.9

There was a statistically significant difference between 1% $CaCO_3$ in the distilled H_2O solution after and before coronal discharge effect, according to Student's t-test at $p < 0.05$ level, with r of 0.964.

Conclusions

Color corona spectral analysis method has been applied for studying $CaCO_3$.

The following conclusions were drawn: a difference in the discharge parameters of H_2O drops was observed for 1% $CaCO_3$ in distilled H_2O before and after coronal discharge effect; there was an increase in electric conductivity and pH studied parameters; the number of OH- hydroxyl groups also increased with higher pH values.
During the coronal discharge process with 1% $CaCO_3$ in a distilled H_2O solution, this study illustrated the increase in the peak of energies distribution function for hydrogen bonds among H_2O molecules f(E) at 877 cm^{-1}, from 32.6 to 44.9 eV^{-1}. These findings have applications for chemical processes with color corona discharge on $CaCO_3$.
There were corona gas discharge effects from the primordial atmosphere to H_2O. In 1952, Miller-Urey experiments were performed with gas discharge effects in laboratory conditions. Twenty organic molecules have been structured from the following inorganic compounds: H_2O, CH_4, NH_3, H_2 and electric discharge [63]. Different scientists have repeated the Miller-Urey experiment.
In 1968, [64] have synthesized porphyrin using a device with U = 12 kV. In 2014, [1] investigated corona discharge and protocells synthesis with the same value [64]. In 2021, [39] published chemical reactions of polar molecules in H_2O with gas discharge conditions. In 2021, [65] have studied Miller-Urey experiment processes in a silica medium with U = 30 kV.

Authors' contributions

Ignat Ignatov: conceived the research paper original idea; collected data; performed experimental work; inserted data or analysis tools; wrote the paper. **Christos Drossinakis**: collected data; performed experimental work; and analyzed data obtained by xperiments. **Alexander I. Ignatov**: collected data; performed experimental work; and wrote the references.

Abbreviations

BoPET: biaxially-oriented polyethylene terephthalate
Ca^{2+}: calcium ions
$CaCO_3$: calcium carbonate
$Ca(HCO_3)_2$: calcium hydrogen carbonate
CH_4: methane
CO_2: carbon dioxide
CO_3^-: carbonate ions
Cu: copper
d: gap length
DNES: differential non-equilibrium spectrum
E: energy (eV)
Em: electromagnetic spectrum
eV: electron volts
f(E): energy distribution spectrum function
FTIR: Fourier transform infrared
H_2: hydrogen
H_2O: water
HCO_3^-: hydrogen carbonate ion

HOH: hydrogen hydroxide
LED: light emitting diode
N: nitrogen
NES: non-equilibrium energy spectrum
NH_3: ammonia
O: oxygen
p: gas pressure
P_{eff}: effective power
r: correlation coeficient
R: electric resistance
U: voltage (kV)
V_B: breakdown voltage

Symbols definition
α: electric pulse slope rate
Δf: frequency change
δ: surface tension
θ: wetting angle
λ: wavelength (nm)
ν: electric frequency
ν̃: wavenumber
λ: wavelength

References

1. Ignatov I, Mosin OV. Kirlian effect in modeling of non-equilibrium conditions with the gas-electric discharge, simulating primary atmosphere. Nanotechnology. Res Pract. 2014;3(3):127-140.
2. Kirlian SD. Patent of SU. 1949;106401.
3. Pehek JO, Kyler HJ, Faust DL. Image modulation in corona discharge photography. Science. 1976;194(4262):263-270. https://doi.org/10.1126/science.968480
4. Antonov A, Yuskesselieva L. Research of water drops with high-frequency electric discharge (Kirlian) effect. Compt Rend Acad Bulg Sci.1968;21(5):34-36.
5. Go DB, Venkattraman A. Microscale gas breakdown: ion-enhanced field emission and the modified Paschen's curve. J Phys D: Appl Phys. 2014;47:503001. https://doi.org/10.1088/0022-3727/47/50/503001
6. Schaffert RM. Electrophotography, The Focal Press, London, N.Y. 1965.
7. Faust D, Gross GL, Kyler HJ et al. Investigation into the reliability of electrophotography. Def Techn Inform Cent. 1975;1:ADA018806.
8. Golovin BM, Fridkin VM, Antonov A et al. Electrophotography of proton beams. Zhur Nauch i Priklad Fot i Kinematografii. 1960;3:402124.
9. Yuskesselieva L, Antonov A. A modification of the electrophotographic method of studying liquid aerosols in the atmosphere. Bulgarska Akademiia na Naukite, Geofizichni Institut, Izvestiia. 1974;20:31-37.
10. Inyushin VM, Grishchenko VS, Vorobyov NA et al. On the biological character of the Kirlian effect – The concept of biological plasma. Alma-Ata: Kazakh State University.1968.

11. Boyers DG, Tiller WA. Corona discharge photography. J Appl Phys. 1973;44:3102-3112. https://doi.org/10.1063/1.1662715
12. Thomas RC. Use of Kirlian photography in fatigue assessment. Defense Technical Information Center. 1975;ADA026349.
13. Cope FM. Magnetoelectric charge states of matter-energy. A second approximation. Part VII. Diffuse relativistic superconductive plasma. Measurable and non-measurable physical manifestations. Kirlian photography. Laser phenomena. Cosmic effects on chemical and biological systems. Physiolog Chem Phys. 1980;12(4):349-355.
14. Ebrahim H, Kirlian WR. Photography – an appraisal. J Audiov Media Medic. 1982;5(3):84-91. https://doi.org/10.3109/17453058209154332
15. Gudakova GZ, Galynkin VA, Korotkov KG. Study of the spectral characteristics of gas-discharge luminescence of microbiological cultures. J Appl Spectrosc. 1988;49:916-920. https://doi.org/10.1007/BF0066278
16. Pesotskaya LA, Ilinchuk IV, Tsybulskaya IV et al. |Kirlian-diagnostika v terapevticheskoi praktike. Likars'ka sprava/Ministerstvo okhorony zdorov'ia Ukraïny. 2004;(5-6):39-43.
17. Kurik MV, Pesotskaya LA, Lapitsky VN et al. About the nature of Kirlian glow of the water. Naukovyi Visnyk Natsionalnoho Hirnychoho Universytetu. 2012;5:86-90.
18. Pesotskaya LA, Glukhova NV, Lapitskiy VN. Analysis of the images of the water drops Kirlian glow. Naukovyi Visnyk Natsionalnoho Hirnychoho Universytetu. 2013;1:91-96.
19. Antonov A. Research of the non-equilibrium processes in the area of allocated systems. Dissertation thesis for degree “Doctor of Physical Sciences”, Blagoevgrad, Sofia. 1995:1-255.
20. Ignatov I, Iliev MT, Gramatikov PS. Education program on Physics and Chemistry for non-equilibrium processes at the interfaces between solid-liquid-gaseous media. Eur J Contemp Educ. 2023;12(3):862-873. https://doi.org/10.13187/ejced.2023.3.862
21. Ignatov I, Antonov A, Neshev N et al. High-frequency coronal discharge, infrared thermography, and visual acuity measurements of bioelectromagnetic influence. Phys Sci Int J. 2021;25(3):18-28. https://doi.org/10.9734/PSIJ/2021/v25i330246
22. Leskowitz E. Cartography of energy medicine: From subtle anatomy to energy physiology. Explorer. 2022;18(2):152-164. https://doi.org/10.1016/j.explore.2020.09.008
23. Sano N, Kawashima T, Fujikawa J et al. Decomposition of organic compounds in water by direct contact of gas corona discharge: Influence of discharge conditions. Ind Eng Chem Res. 2002;41(24):5906-5911. https://doi.org/10.1021/ie0203328
24. Ignatov I, Antonov A, Neshev N et al. Color coronal spectral analysis of bioelectrical effects of humans and water. Contemp Eng Sci. 2021;14(1):61-72. https://doi.org/10.12988/ces.2021.91781
25. Glukhova N, Khilov V, Kharlamova Yu et al. Integrated assessment of the state of sewage mine waters based on gas-discharge radiation method. E3S Web Confer. 2020;201:01032. https://doi.org/10.1051/e3sconf/202020101032

26. Ewing RG, Waltman MJ. Production and utilization of CO_3^- produced by a corona discharge in the air for atmospheric pressure chemical ionization. Spectrometry. 2014;296(1-3):53-48. https://doi.org/10.1016/j.ijms.2010.08.024
27. Kaufmann G, Dreybrodt W. Calcite dissolution kinetics in the system $CaCO_3$–H_2O–CO_2 at high undersaturation. Geochem Cosmochim Acta. 2007;71(6):1398-1410. https://doi.org/10.1016/j.gca.2006.10.024
28. Ignatov I, Mosin OV. Isotopic composition of water and its temperature in modeling of primordial hydrosphere experiments. Eco-Euro. 2012;1:62.
29. Falk M. The frequency of the HOH bending is fundamental in solids and liquids. Spectrochim Acta: Part A Mol Spectrosc. 1984;40:43-48. https://doi.org/10.1016/0584-8539(84)80027-6
30. Vinh Tran H, Dai Tran L, Dinh Vu H et al. Facile surface modification of nano-precipitated calcium carbonate by adsorption of sodium stearate in aqueous solution. Colloids Surf A Physicochem Eng Asp. 2010;366:95-103. https://doi.org/10.1016/j.colsurfa.2010.05.029
31. Joksa AA, Komarovska L, Ubele-Kalnina D et al. Role of carbonate on the crystallization and processing of amorphous calcium phosphates. Materialia. 2023;27:101627. https://doi.org/10.1016/j.mtla.2022.101672
32. Todorov S, Damianova A, Sivriev I et al. Water energy spectrum method and investigation of the variations of the H-bond structure of natural waters. Compt Rend Acad Bulg Sci. 2008;61:857-862.
33. Mehandjiev D, Ignatov I, Neshev N et al. History-dependent hydrogen bonds energy distributions in NaCl aqueous solutions undergoing osmosis and diffusion through a ceramic barrier. J Chem Technol Metall. 2023;58(2):340-346.
34. Iliev MT, Huether F, Ignatov I et al. Education of students on Physics and Chemistry with effects of water filtration. Modeling of water clusters and hexagonal structures. Eur J Contemp Educ. 2023;12(4):1546-1560. https://doi.org/10.13187/ejced.2023.4.1546
35. Ignatov I, Iliev MT, Gramatikov P et al. Non-equilibrium processes in the atmosphere, water, and reactions with calcium carbonate in the environment. J Chem Technol Metall. 2023;58(6):1100-1106.
36. Ignatov I, Huether F, Neshev N et al. Research of water molecules cluster structuring during *Haberlea rhodopensis*. Friv Hydrat Plants. 2022;11(19):2655. https://doi.org/10.3390/plants11192655
37. Ignatov I, Valcheva N. Physicochemical, isotopic, spectral, and microbiological analyses of water from glacier Mappa, Chilean Andes. J Chil Chem Soc. 2023;68(1):5802-5906.
38. Ignatov I. Energy Biomedicine. ICH, Munich. 2007;1:136.
39. Ignatov I. Origin of life and living matter in hot mineral water and properties of polar molecules in the primary hydrosphere and hydrothermal ponds. Uttar Pradesh J Zoolog. 2021;42(6):37-52.
40. Ignatov I, Mosin OV, Niggli H et al. Methods for registering non-ionizing radiation emitted from the human body. Eur Rev Chem Res. 2015;3(1):4-24.
41. Antonov A. An optical method version for determination of the wetting angle of liquids. Compt Rend Acad Bulg Sci. 1984:37:1199.

42. Antonov A, Yuskesselieva L, Teodossieva I. Influence of ions on the structure of water under conditions far away from equilibrium. Physiologie. 1989;26:2552.
43. Todorova L, Antonov A. Note on the drop evaporation method for the study of water hydrogen bond distribution: I. An application for filtration. Compt Rend Acad Bulg Sci. 2000;53:43-46.
44. Luck W. A model of hydrogen-bonded liquids. Angewandte Chemie. 1980;19:28-41. https://doi.org/10.1002/anie.198000281
45. Kontogeorgis GM, Hoster A, Kottaki A et al. Water structure, properties and some applications – a review. Chem Thermodynam Therm Analyt. 2022;6:100053. https://doi.org/10.1016/j.ctta.2022100053
46. Vega LF, Lovell F. Review and new insights into the application of molecular-based equations of state to water and aqueous solutions. Fluid Ph Equilib. 2016;416;150-173. https://doi.org/10.1016/j.fluid.2016.01.024
47. Aparicio-Martínez S, Hall K. Phase equilibria in water containing binary systems from molecular-based equations of state. Fluid Phase Equilib. 2007;254:112-125. https://doi.org/10.1016/j.fluid.2007.02.030
48. Clark G, Haslam A, Galindo A et al. Developing optimal Wertheim - like models of water for use in statistical associating fluid theory (SAFT) and related approaches. Mol Phys. 2010;104:3561-3581. https://doi.org/10.1080/00268970601081475
49. Zhang B, Kim J, Lee T Ch. Behavior of an evaporating water droplet on a lubricant-impregnated nano-structured surface. Exp Therm Fluid Sci. 2018;96:216-223. https://doi.org/10.1016/j.expthermflusci.2018.02.035
50. Luzar A, Svetina S, Žekš B. The contribution of hydrogen bonds to the surface tension of water. Chem Phys Lett. 1983;96:485-490. https://doi.org/10.1016/0009-2614(83)80737-4
51. Gramatikov PS, Antonov AS. On the two conditions model of water structure. Compt Rend Acad Bulg Sci. 1997;50(3):13-16.
52. Gramatikov P, Antonov A, Gramatikova M. Study of the properties and structure variations of water systems under the stimulus of outside influences. Fresenius Z Analy Chem. 1992;343:134-135. https://doi.org/10.1007/BF00332070
53. Todorov S, Damianova A, Antonov A et al. Investigations of natural waters spectra from the lakes of Rila mountain national park. Compt Rend Acad Bulg Sci. 2010;63:555-560.
54. Ignatov I, Gluhchev G, Neshev N et al. Structuring of water clusters depending on the energy of hydrogen bonds in electrochemically activated waters Anolyte and Catholyte. Bulg Chem Commun. 2021;53:234-239.
55. Boteva S, Kenarova G, Radeva I et al. Community dynamics of pelagic bacteria in the high mountain lake Bubreka, Rila mountain. Bulgaria. Biotechnol Biotech Equip. 2014;25(4):2620-2626. https://doi.org/10.5504/BBEQ.2011.0063
56. Neshev N, Ignatov I, Toshkova R et al. Hydrogen bonds energy distribution and information-theoretic analysis of blood serum from hamsters with experimental Graffi tumor. Libri Oncol. 2022;50(2-3):52-61. https://doi.org/10.20471/LO.2022.50.02-03.10

57. Yu T, Li Q, Hu H et al. Molecular dynamics simulation of the interfacial wetting behavior of brine/sandstone with different salinities. Collo Surf: Physicochem Eng Asp. 2022;632:127807. https://doi.org/10.1016/j.colsurfa.2021.127807
58. Yitian G, Hongwei F, Ni KA. Hierarchical clustering method of hydrogen bond networks in liquid water undergoing shear flow. Scient Rep. 2021;11:9542. https://doi.org/10.1038/s41598-021-88810-7
59. Glukhova N. Development of express-evaluation method of water biological properties. East Europ J Enterpr Technol. 2014;6(5):18-25. https://doi.org/10.15587/1729-4061.2014.31546
60. Panayotov D, Zdravkova V, Lagunov O et al. Capturing CO_2 by *Ceria-zirconia* nanomaterials of different origins. Physic Chemi Chem Phys. 2023;(25)26:17154-17175. https://doi.org/10.1039/d3cp00896g
61. Ignatov I, Popova TP, Petrova T et al. Physicochemical parameters and in vitro antimicrobial effects of water filtrated with nano-structured carbonaceous shungite. J Chem Technol Metall. 2022;57(5):937-947.
62. Messer JK, De Lucia FC, Helminger P. The pure rotational spectrum of water vapor–A millimeter, submillimeter, and far infrared analysis. Int J Infrared Milli Waves. 1983;4:505-539. https://doi.org/10.1007/BF01009392
63. Miller SL. Production of amino acids under possible primitive earth conditions. Science. 1953;117(3046):528-529.
65. Ignatov I, Mosin OV. Hot mineral water with more deuterium for origin of life and living matter. Process of formation of stromatolites. J Health Med Nurs. 2014;6:1-24.
66. Criado-Reyes J, Bizzarri BM, Garcia-Ruiz JM et al. The role of borosilicate glass in Miller-Urey experiment. Scientif Rep. 2021;11:21009.